AGU PUBLICATIONS

JGR

Journal of Geophysical Research: Atmospheres

RESEARCH ARTICLE
10.1002/2013JD021060

Special Section:
The Geoengineering Model Intercomparison Project

Arctic sea ice and atmospheric circulation under the GeoMIP G1 scenario

John C. Moore[1], Annette Rinke[1,2], Xiaoyong Yu[1], Duoying Ji[1], Xuefeng Cui[1], Yan Li[3], Kari Alterskjær[4], Jón Egill Kristjánsson[4], Helene Muri[4], Olivier Boucher[5], Nicolas Huneeus[5], Ben Kravitz[6], Alan Robock[7], Ulrike Niemeier[8], Michael Schulz[9], Simone Tilmes[10], Shingo Watanabe[11], and Shuting Yang[12]

[1]State Key Laboratory of Earth Surface Processes and Resource Ecology, College of Global Change and Earth System Science, Beijing Normal University, Beijing, China, [2]Alfred Wegener Institute Helmholtz Centre for Polar and Marine Research, Potsdam, Germany, [3]College of Atmospheric Science, Lanzhou University, Lanzhou, China, [4]Department of Geosciences, University of Oslo, Oslo, Norway, [5]Laboratoire de Météorologie Dynamique, IPSL, CNRS/UPMC, Paris, France, [6]Atmospheric Sciences and Global Change Division, Pacific Northwest National Laboratory, Richland, Washington, USA, [7]Department of Environmental Sciences, Rutgers University, New Brunswick, New Jersey, USA, [8]Max Planck Institute for Meteorology, Hamburg, Germany, [9]Norwegian Meteorological Institute, Oslo, Norway, [10]National Center for Atmospheric Research, Boulder, Colorado, USA, [11]Japan Agency for Marine-Earth Science and Technology, Yokohama, Japan, [12]Danish Climate Centre, Danish Meteorological Institute, Copenhagen, Denmark

Key Points:
- Analysis of eight ESM focused on Arctic sea ice and feedback
- Response of Arctic to G1 geoengineering shows clear regional differences
- Sea ice is far different in detail under G1 than in pre industrial

Supporting Information:
- SI description
- Table S1
- Table S2
- Table S3
- Figure S1
- Figure S2
- Figure S3
- Figure S4
- Figure S5
- Figure S6
- Figure S7
- Figure S8
- Figure S9

Correspondence to:
X. Cui,
xuefeng.cui@bnu.edu.cn

Citation:
Moore, J. C., et al. (2014), Arctic sea ice and atmospheric circulation under the GeoMIP G1 scenario, *J. Geophys. Res. Atmos.*, *119*, 567–583, doi:10.1002/2013JD021060.

Received 23 OCT 2013
Accepted 30 DEC 2013
Accepted article online 3 JAN 2014
Published online 29 JAN 2014

Abstract We analyze simulated sea ice changes in eight different Earth System Models that have conducted experiment G1 of the Geoengineering Model Intercomparison Project (GeoMIP). The simulated response of balancing abrupt quadrupling of CO_2 (abrupt4xCO2) with reduced shortwave radiation successfully moderates annually averaged Arctic temperature rise to about 1°C, with modest changes in seasonal sea ice cycle compared with the preindustrial control simulations (piControl). Changes in summer and autumn sea ice extent are spatially correlated with temperature patterns but much less in winter and spring seasons. However, there are changes of ±20% in sea ice concentration in all seasons, and these will induce changes in atmospheric circulation patterns. In summer and autumn, the models consistently simulate less sea ice relative to preindustrial simulations in the Beaufort, Chukchi, East Siberian, and Laptev Seas, and some models show increased sea ice in the Barents/Kara Seas region. Sea ice extent increases in the Greenland Sea, particularly in winter and spring and is to some extent associated with changed sea ice drift. Decreased sea ice cover in winter and spring in the Barents Sea is associated with increased cyclonic activity entering this area under G1. In comparison, the abrupt4xCO2 experiment shows almost total sea ice loss in September and strong correlation with regional temperatures in all seasons consistent with open ocean conditions. The tropospheric circulation displays a Pacific North America pattern-like anomaly with negative phase in G1-piControl and positive phase under abrupt4xCO2-piControl.

1. Introduction

The most rapid temperature rises over the twentieth century have taken place in the Arctic [e.g., *Richter-Menge and Overland*, 2010]. The rising temperatures have been commensurate with a rapid decline in sea ice extent in all seasons. The expected warming over the 21st century is also expected to be greatest in the Arctic with estimates that the Arctic Ocean may become ice free in September as early as in the 2030s [*Wang and Overland*, 2012]. In general, all climate models have predicted a slower decline in sea ice extent than has been observed in recent decades, although the latest Coupled Model Intercomparison Project Phase 5 (CMIP5) multimodel ensemble mean is more consistent with the observations than earlier models [*Stroeve et al.*, 2012].

Observational evidence links the decline in Arctic summer sea ice extent with atmospheric circulation responses in the following months [e.g., *Overland and Wang*, 2010; *Liu et al.*, 2012; *Francis and Vavrus*, 2012; *Screen et al.*, 2013]. Recently, model results [*Rinke et al.*, 2013] have supported the observational hypothesis that this mechanism could lead to anomalous cold European and Asian winters [*Honda et al.*, 2009; *Petoukhov and Semenov*, 2010; *Cohen et al.*, 2012; *Jaiser et al.*, 2012]. It has also been pointed out that winter sea ice extent directly affects the winter atmospheric circulation through the change in cyclone tracks [*Inoue et al.*, 2012; *Tang et al.*, 2013].

The reduction of the sea ice cover on the Arctic Ocean in summer and autumn is expected to have considerable impacts farther afield than the Arctic region, as changes in albedo and regional atmospheric conditions affect large-scale Rossby waves and global teleconnection patterns [*Dethloff et al*., 2006; *Budikova*, 2009].

The removal of sea ice from the Arctic has also led to considerable changes in the local way of life for the indigenous peoples of the Arctic, who can no longer pursue traditional hunting and fishing without sea ice nor (in several cases) inhabit their villages, as the removal of ice leads to increased coastal erosion [e.g., *Arctic Human Development Report* (*AHDR*), 2004]. An open sea instead of multi-annual sea ice cover has opened new shipping routes in the Arctic, in response to the vast increase in trade between Asia and Europe. The reduced sea ice also opens more of the Arctic Ocean to fossil fuel exploitation, which itself will eventually enhance global warming [e.g., *Arctic Monitoring and Assessment Programme*, 2007].

In this paper we examine how the use of geoengineering may combat the dramatic climate changes expected in the Arctic. We make use of eight models participating in Geoengineering Model Intercomparison Project (GeoMIP) that provide sea ice data for the G1 scenario [*Kravitz et al*., 2011a]. The G1 scenario has climate models balance an abrupt quadrupling of CO_2 with an insolation reduction so as to balance the top-of-the-atmosphere radiative forcing. G1 is a completely artificial experiment meant to provide large climate responses to the very large imposed forcings and is not meant to be interpreted as a realistic geoengineering scheme. Thus, the results presented here should be interpreted as extreme responses that may help to interpret the results of more "realistic" experiments.

Previous work with the G1 scenario shows that while the global temperatures are well constrained to preindustrial levels, the polar regions are relatively warmer by approximately 0.8°C, while the tropics relatively cooler by approximately 0.3°C [*Kravitz et al*., 2013a]. Without the concomitant shortwave insolation reduction, the greenhouse gas forcing under G1 would cause average Arctic temperatures to rise by about 10°C. Under G1, the temperature increase is larger in the winter than the summer and hence may have a smaller impact on seasonal melt of sea ice and snow cover. The GeoMIP models show largest differences in surface air temperatures over the Arctic and Southern Ocean, which might be because of intermodel differences in sea ice feedback processes. Thus, one may expect that the Arctic will be slightly warmer in the G1 scenario with reduced snow cover and sea ice concentrations as compared to the preindustrial period but considerably cooler than the corresponding longwave forcing experiment (abrupt4xCO2), where the greenhouse gas forcing is not compensated by a shortwave radiative forcing. However, one may also expect changes in regional and large-scale atmospheric circulation patterns as a result of the regional differences in radiative forcing and temperatures compared with the preindustrial. Investigating sulfate geoengeneering, *McCusker et al*. [2012] emphasize the role of ocean dynamics and atmospheric circulation for the polar climate response.

In this paper we examine the ability of G1 to maintain the preindustrial (piControl) Arctic sea ice and atmospheric circulation. Key questions we investigate are as follows: Is G1 able to offset the dramatic sea ice loss and the significant changes in atmospheric circulation occurring under abrupt4xCO2? What regional differences in sea ice and circulation patterns are manifested in G1 compared with piControl? What are the mechanisms for such regional sea ice differences? To diagnose mechanisms we need to look at the differences between the three experiments (piControl, abrupt4xCO2, and G1), and therefore, we compare G1-piControl with abrupt4xCO2-piControl. We focus in our analysis on sea ice, surface temperatures, and atmospheric circulation since the surface temperatures reveal near-surface thermal conditions and relate to sea ice via the Arctic amplification and ice-albedo feedback, while sea level pressure characterizes near-surface atmospheric dynamics that impact sea ice.

2. Analysis Methods

We use data from eight GeoMIP model groups that provided sea ice concentrations (BNU-ESM, CCSM4, EC-EARTH, GISS-E2-R, IPSL-CM5A-LR, MIROC-ESM, MPI-ESM, and NorESM1-M; Table S1 in the supporting information). The model setup is the same as described by other articles in this issue, that is, the simulations in each model are initiated from a preindustrial control run which has reached steady state, denoted as piControl, which is the standard CMIP5 name for this experiment [*Taylor et al*., 2012]. Our reference simulation, denoted abrupt4xCO2, is one in which CO_2 concentrations are instantaneously quadrupled from the

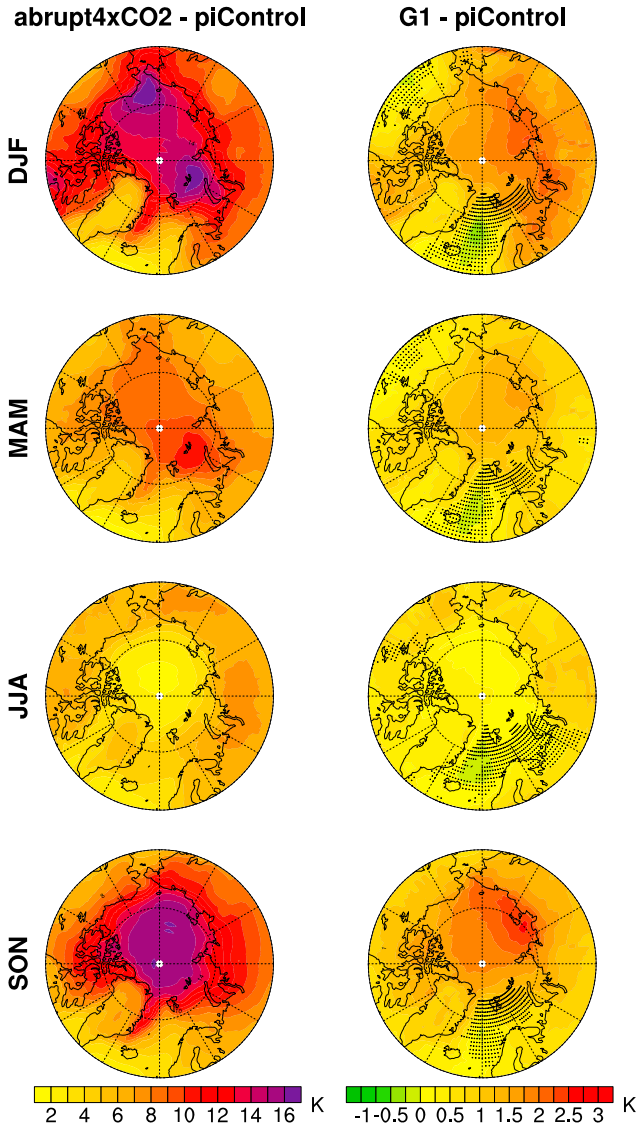

Figure 1. Multimodel ensemble mean seasonal surface air temperature anomalies (K) for the Arctic region for (left) abrupt4xCO2-piControl and (right) G1-piControl. Stippling shows regions where less than six of eight models agree on the sign of the response. Figure S1 shows the individual model results.

control run. This experiment implies an atmospheric CO_2 concentration of nearly 1140 ppm. Experiment G1 involves an instantaneous reduction of insolation simultaneous with this CO_2 increase such that top-of-atmosphere radiation differences between G1 and piControl are no more than 0.1 W m^{-2} for the first 10 years of the 50 year experiment [*Kravitz et al.*, 2011a, 2011b]. The amount of solar radiation reduction is model dependent but does not vary during the course of the simulation.

The coupled models in general differ by their resolution, components, and parameterizations. Also, the sea ice representation in the different models vary reasonably widely in both resolution and sea ice physics included (Table S1) [*Massonnet et al.*, 2012]. Therefore, we choose to not only show ensemble means but also display results of individual models and discuss the relationships of the sea ice with atmospheric variables. This allows us to examine specific mechanisms that may both drive sea ice change and be driven by the new sea ice distribution. We use the complete 50 year simulation period of G1 and the longest *piControl* and abrupt4xCO2 experiments to calculate anomalies. There are some feedback related to global temperature change that will not be present in the first few years of the simulation but operative later. Sea ice is a very small part of the total energy content of the climate system, which responds very rapidly to forced change [*Bindoff et al.*, 2007],

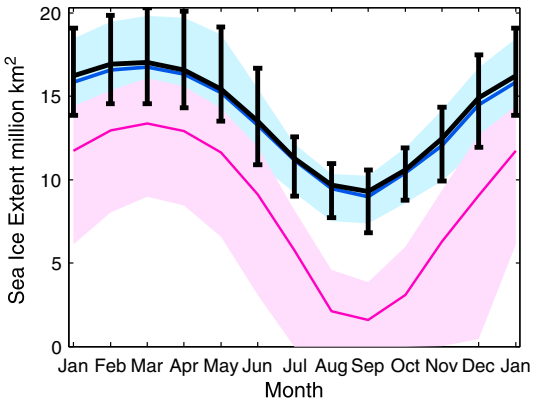

Figure 2. Multimodel ensemble mean monthly sea ice extent (million km^2; following the standard definition of area of the ocean with sea ice concentration of at least 15%) for abrupt4xCO2 (red), piControl (black), and G1 (blue). The ensemble mean is the thick line, light blue and pink bands show the full range of variability of across-model mean monthly values for G1 and abrupt4xCO2, respectively, and error bars shows the piControl across-model range.

consistent with very variable annual sea ice extent. Climate models used to test summer Arctic sea ice recovery after either sudden artificial removal find that sea ice returns within a few years [*Schröder and Connolley*, 2007], consistent with very variable annual sea ice extent. Hence, we use the full 50 year simulation to extract the highest signal-to-noise ratio in the simulations.

3. Results

3.1. Surface Air Temperatures

Figure 1 shows the ensemble mean seasonal temperature anomalies for the eight models we analyze. Arctic temperatures in G1 are about 2°C higher than piControl in winter and about 1°C higher in summer. This is a far smaller change than the abrupt4xCO2 increases which average about 10°C annually. However, local temperature changes are much greater than these means, with some regions being up to 6°C warmer than piControl under G1, particularly in autumn and winter, and a few places being noticeably cooler by up to 2°C, especially North Greenland in summer. Summer is, in general, the coolest season under G1 relative to piControl. Similar as with abrupt4xCO2 and consistently across the models, the maximum warming in G1 relative to piControl is found over the Barents Sea area in winter (Figure S1) and is related to the sea ice reduction that we will discuss next.

3.2. Sea Ice Extent and Concentrations

Figure 2 shows the seasonal cycle of sea ice extent. The across-model scatter for each of the three experiments is greater at maximum extent in March than at minimum in September (scatter of ~ 6 and 3 million km^2, respectively, for G1). While the ensemble average shows dramatic reductions in sea ice extent for the abrupt4xCO2 experiment compared with piControl (five of eight models show a summertime ice-free Arctic), the G1 experiment shows only a slight decrease in extent relative to piControl so that it maintains the preindustrial sea ice extent of ~ 9 million km^2 in September and ~ 17 million km^2 in March. The timings of the maximum and minimum sea ice extents remain in March and September, respectively, despite the large differences in forcing across the three experiments. Table 1 also shows that sea ice total area in the models decreases much more in September than in March, and this difference reflects a relative increase in first-year ice and decrease in multiyear ice in almost all models under both abrupt4xCO2 and G1. Even though the total ice area under G1 is almost the same as that of piControl (a decrease of 3% in the G1 ensemble mean annual ice area, relative to piControl), the loss of multiyear ice (−7%) suggests a thinner and more mobile ice cover in G1 than under piControl conditions (Table 1).

Table 1. Relative Sea Ice Area Change for Multiyear and First-Year Sea Ice Following *Zhang and Walsh* [2006]

	abrupt4xCO2			G1		
	Relative Change From piControl (%)			Relative Change From piControl (%)		
Model	Annual	Multiyear (September)	First Year (March–September)	Annual	Multiyear (September)	First Year (March–September)
BNU-ESM	−54	−93	22	−8	−23	12
CCSM4	−35	−84	57	−6	−13	4
EC-EARTH	−58	−87	19	−4	−4	−4
GISS-E2-R	−29	−96	33	1	11	−8
IPSL-CM5A-LR	−42	−81	23	−1	−4	4
MIROC-ESM	−82	−97	−37	−1	−6	4
MPI-ESM-LR	−54	−94	21	−2	−7	4
NorESM1	−37	−82	65	−1	−3	2
Ensemble mean	−48	−89	25	−3	−7	2

Therefore, we may conclude that the G1 forcing achieves the target of maintaining preindustrial conditions for Arctic sea ice extent. However, this slight total area change may mask considerable regional changes in sea ice if reorganization of atmospheric and ocean circulation occurs under the G1 forcing. Since sea ice is challenging for models to simulate because of a variety of complex processes (e.g., ice and snow cover melt/growth, ice transport, rafting, ridging, and subgrid cell features), regional responses in sea ice concentration show pronounced across-model scatter. Accordingly, in Figure 3 we investigate maps of sea ice concentrations showing the results from all the models for the two sets of anomalies abrupt4xCO2-piControl and G1-piControl, and we illustrate the yearly behavior by showing the conditions in the annual minimum represented by the September maps and the annual maximum extent with the March maps. When reading the difference plots it should be noted that a difference of 20% in March could mean that sea ice concentrations are reduced from, for example, 80–60% (over the central Arctic Ocean), or it could mean that a 20% cover is reduced to zero (marginal seas). For reference, Figure S2 shows the actual sea ice concentration maps for piControl, G1, and abrupt4xCO2 for March and September. The seasonal maps of the differences abrupt4xCO2-piControl and G1-piControl for all models are shown in Figure S3. It has been noted previously that some models (including GISS-E2-R used here) have unrealistic sea ice thickness distribution, while others (including IPSL-CM5A-LR and NorESM1-M) overestimate the extent of sea ice in historical simulations [*Maslowski et al*., 2012]. Here we see that GISS-E2-R and IPSL-CM5A-LR overestimate March sea ice extent in piControl.

It is immediately obvious that abrupt4xCO2 forcing reduces sea ice concentration by 90% in many models and regions during summer and autumn seasons. Five out of the eight models are practically ice free under abrupt4xCO2 in September (Figure 3). The largest March sea ice reductions common to models are in the Barents, Kara, and Greenland Seas. This can be related to largest warming in these seas (Figure 1).

In contrast, the G1-piControl anomalies show sea ice concentration changes of less than about ±20%. Thus, G1 returns the sea ice concentrations almost to preindustrial conditions and prevents the dramatic sea ice loss seen under abrupt4xCO2. There is a clear correlation between anomalies of sea ice concentration and surface temperatures (Figures 1, 3, S1, and S3 and Table S2). In most regions and all models (except GISS-E2-R), G1 simulates reduced sea ice concentrations but with increased sea ice concentration in some places. The spatial patterns of regional sea ice concentration decrease/increase differ between the individual models, which likely reflect changes in regional winds and ocean currents (see section 4 for detailed discussion).

In March, models behave differently in the Barents Sea (some show decreases, and some show increases) under G1. Our results show that the sign of the sea ice cover change in the Barents Sea under G1 is related to the ice simulation in that region in piControl: models which simulate small ice cover in piControl simulate increased ice cover there in G1, and models which simulate large ice extent in piControl simulate decreased ice there in G1.

Figure 3 further indicates that many models show a striking tongue of increased sea ice concentration in the Greenland Sea under G1 in March. This feature is coincident with a region of reduced surface air temperatures and a larger area of lesser temperature rise (Figure S1) and also partly reflects a change in the ice drift path along the east Greenland current and the westerly Jan Mayen current. The same two mechanisms (cooling and sea ice drift) are also seen under abrupt4xCO2 and explain the occurrence of local sea ice increase in Greenland Sea or north Labrador Sea in some models (see section 4 for more details).

In September, the Laptev, East Siberian, Chukchi, and Beaufort Seas appear to have relatively less ice cover, while in part more is present in the Barents, Greenland, and Nordic Seas regions. This is a robust feature across the eight models. These regional summer sea ice concentration changes under G1, compared to piControl, are related to the regional temperature changes as well as with regional changes in atmospheric wind and ice drift (see section 4 for more details).

Figure 4 shows that G1 also maintains the pattern of piControl sea ice cover interannual variability (i.e., the year-to-year changes of seasonal means calculated by the seasonal standard deviation), with high variability in March and September along the sea ice edges. Thus, in general, sea ice variability in the marginal ice zone under G1 is similar as in piControl and far different from abrupt4xCO2, which shows higher sea ice cover variability in September than in March, associated with the thin ice located in the central Arctic Ocean. The increase/decrease of sea ice concentration along the North Atlantic sea ice margins in G1 compared to

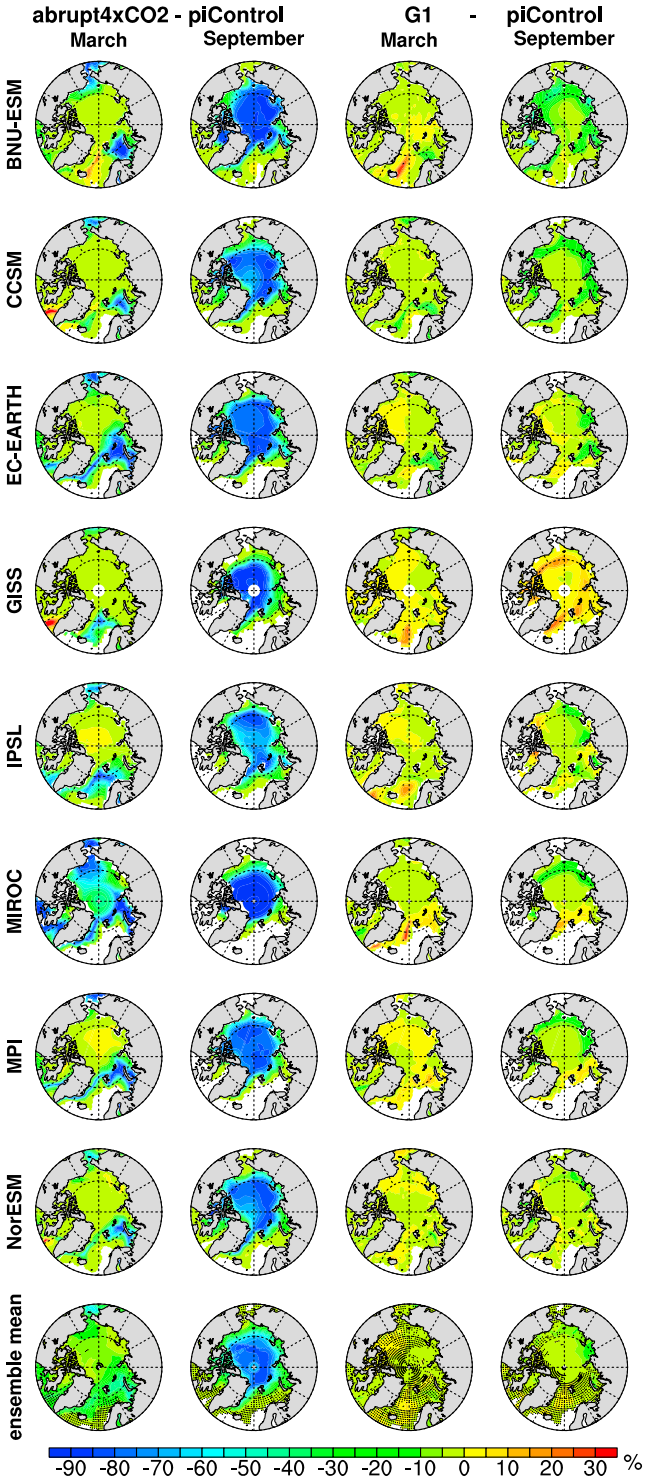

Figure 3. Model simulations of March (maximum sea ice extent) and September (minimum extent) sea ice concentration anomalies (%) for abrupt4xCO2-piControl and G1-piControl for the eight models we analyze here. The ensemble mean has stippling where less than six of eight models agree on sign of change. Figure S2 shows the actual sea ice concentration map for each experiment.

piControl seen in the different models (Figure 3) is, to some extent, associated with decreased/increased variability in sea ice concentrations from year-to-year (Figure S4) and suggestive of variability in warm air advection (associated with cyclone activity) and water inflow (associated with the Norwegian Atlantic, East Greenland, and Jan Mayen currents), as discussed later in section 4.2.

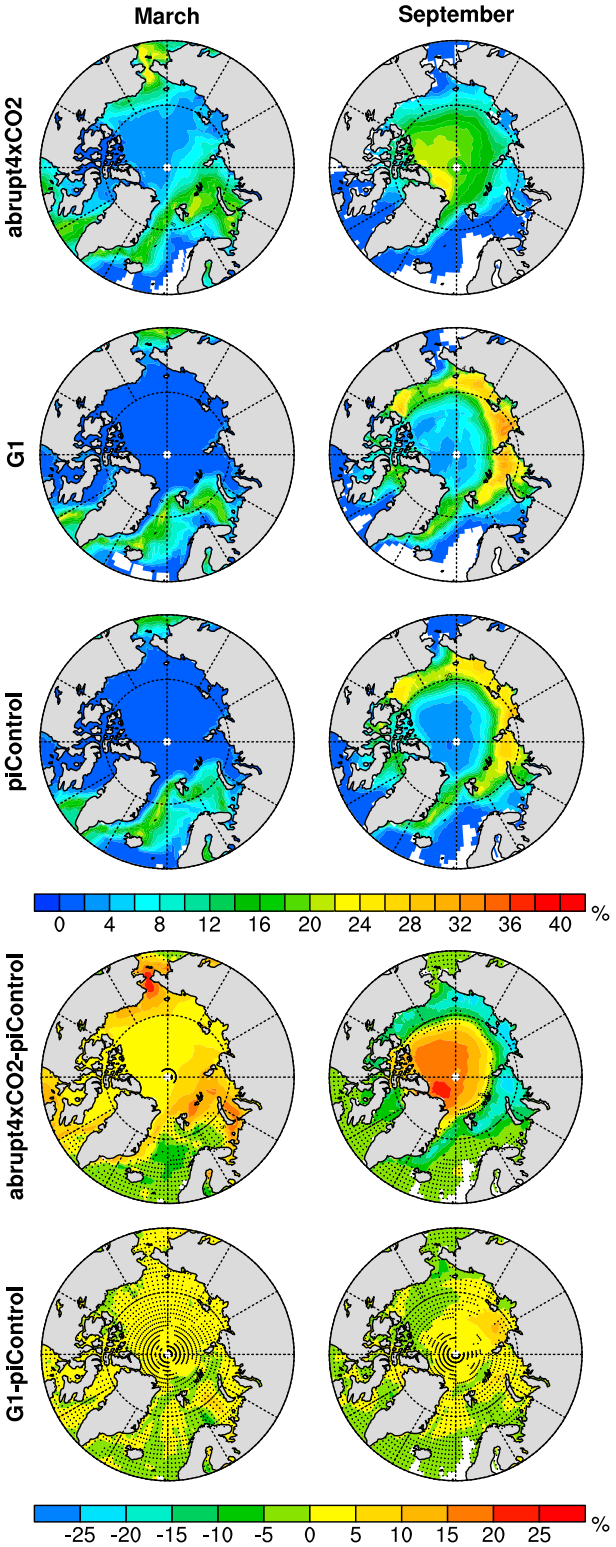

Figure 4. Multimodel ensemble mean standard deviation of March and September sea ice concentration (%) for abrupt4xCO2, G1, and piControl and the anomalies for abrupt4xCO2-piControl and G1-piControl. Stippling shows where less than six of eight models agree on sign of change. Figure S4 shows the individual model results.

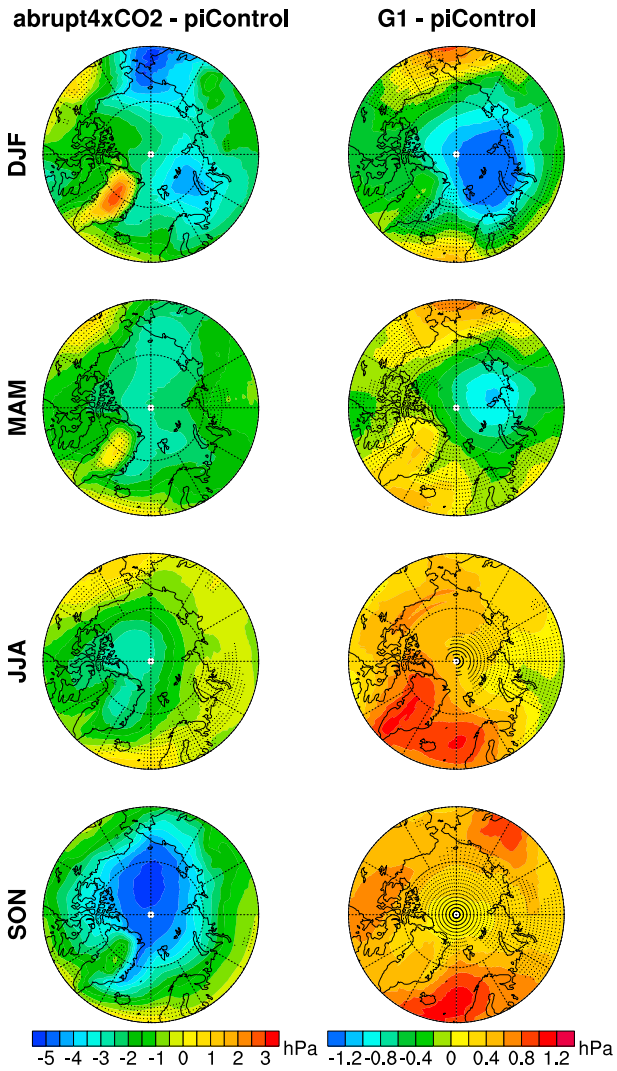

Figure 5. Multimodel ensemble mean seasonal sea level pressure anomalies (hPa) for (left) abrupt4xCO2-piControl and (right) G1-piControl. Stippling shows regions where less than six of eight models agree on the sign of the response. Figure S5 shows the individual model results.

3.3. Atmospheric Circulation

The changes in sea ice concentration (section 3.2; Figures 3 and S3) are expected to force regional changes in atmospheric circulation, via changed surface temperature, turbulent heat fluxes, and baroclinicity, which affects synoptic cyclone activity which in turn interacts with the large-scale circulation (see the review by *Budikova* [2009, and references therein]). Maps of sea ice and temperature are correlated with each other observationally [*Ogi et al*., 2008] and in models (Tables S2 and S3). Here we examine the mean sea level pressure (SLP) describing the near-surface atmospheric dynamics and the atmospheric circulation at higher levels. For the latter we analyze the changes in the geopotential height at 500 hPa and 200 hPa and the upper tropospheric wind at 200 hPa (the height of the jets).

SLP anomalies (Figure 5) resemble the temperature pattern (Figure 1) with warming correlated with a decrease of SLP, particularly in winter and autumn. Under abrupt4xCO2, the strongest negative SLP anomalies (up to −5 hPa in the ensemble mean and up to −8 hPa in individual models; Figure S5) are very consistent among the models and located over the Barents/Kara Seas and Bering/Chukchi/East Siberian Seas regions in winter and over the Arctic Ocean in autumn. This is a manifestation of the strongest warming and reduction in sea ice under abrupt4xCO2. The G1 experiment basically maintains the seasonal SLP of piControl. The anomalies of G1-piControl are within ±1.5 hPa in the ensemble mean (within ±3 hPa in individual models;

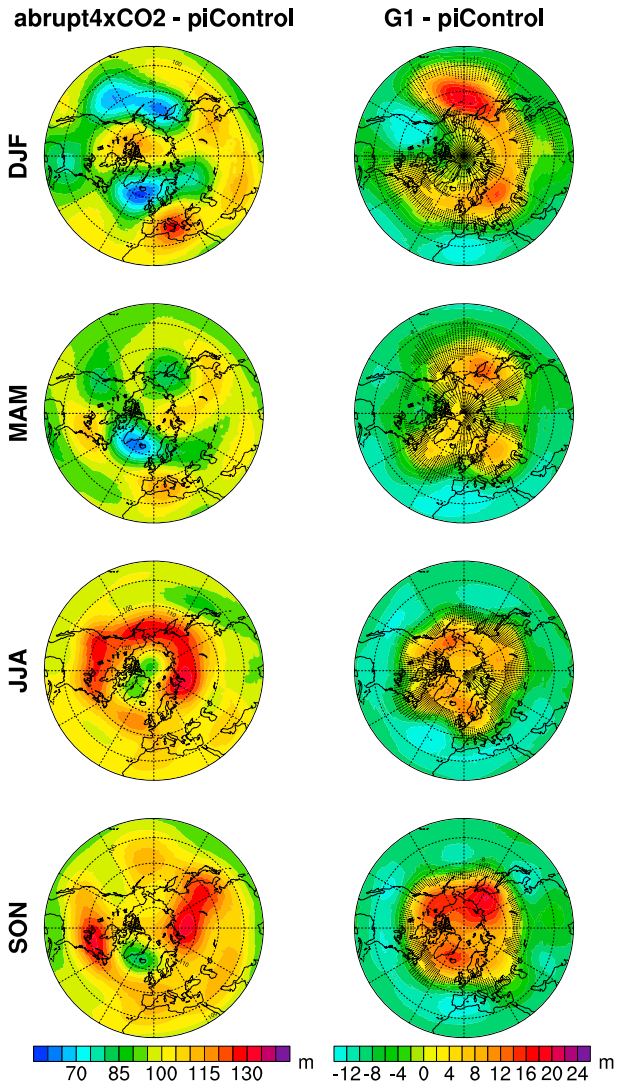

Figure 6. Same as Figure 5 but for the 500 hPa geopotential height (m). Figure S6 shows the individual model results.

Figure S5), i.e., about half of magnitude of those seen in abrupt4xCO2-piControl. But in some regions the anomalies are comparable to each other, namely over the Kara/Laptev Seas area in spring and over the northern North Atlantic and Barents Sea in summer and autumn. This highlights the importance of circulation changes in G1, even though the surface air temperature anomalies are one tenth as large as the abrupt4xCO2 anomalies. In G1, most models agree on a reduced SLP over the Arctic and an increase over parts of the lower latitudes (with the largest increase in Bering Sea and northern North Atlantic) in winter and spring, compared with piControl, although there is a large scatter among the individual model regional response patterns (Figure S5). The consistent, across-model SLP reduction over the Barents/Kara Seas in winter in G1 (Figures 5 and S5) is associated with the regional sea ice reduction and warming, as in abrupt4xCO2 (Figures 1, 3, S1, and S3). In summer and autumn, the SLP anomalies G1-piControl show a general increase, with a consistent, across-model regional maximum over the northern North Atlantic region.

At higher levels in the atmosphere, the geopotential heights (at 500 hPa and 200 hPa) show a general significant increase under abrupt4xCO2 with a rather zonally symmetric structure in summer and a much stronger, zonally asymmetric component displaying a pronounced wave structure in winter (Figures 6 and 7). In both abrupt4xCO2 and G1 experiments the models with weaker warming (Figure S1) show weaker changes in atmospheric circulation patterns (Figures S6 and S7). The G1-piControl 500 hPa geopotential height anomalies are approximately one third of the magnitude of the abrupt4xCO2-piControl changes and

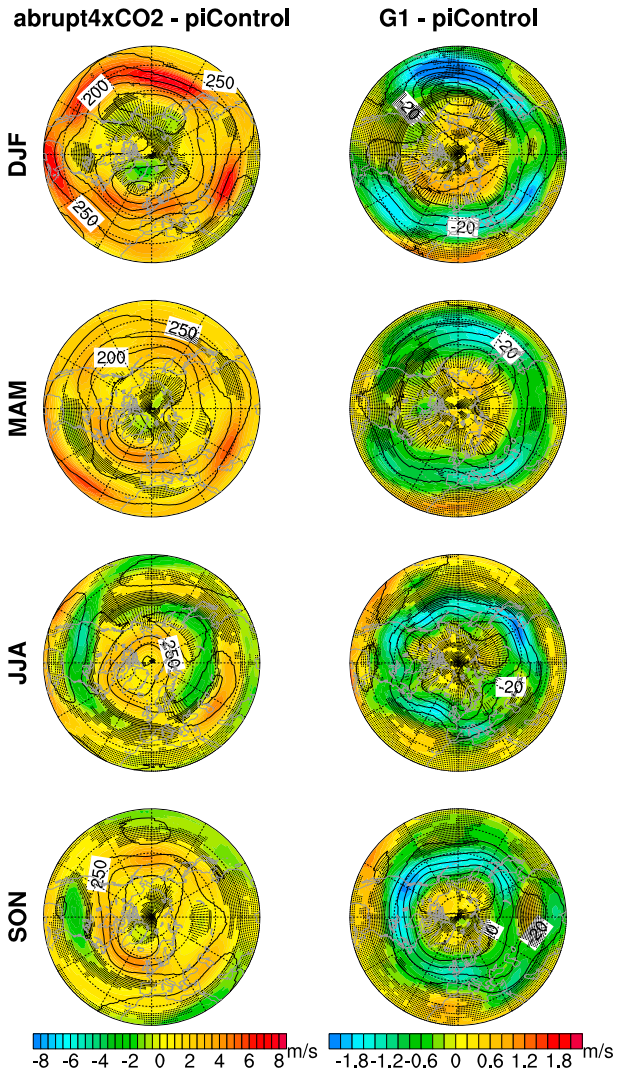

Figure 7. Multimodel ensemble mean seasonal 200 hPa wind speed anomalies (m/s; color) for (left) abrupt4xCO2-piControl and (right) G1-piControl. Stippling shows regions where less than six of eight models agree on the sign of the wind speed response. The black isolines show the 200 hPa geopotential height anomalies (m) with intervals of 25 m in Figure 7 (left; abrupt4xCO2-piControl) and intervals of 10 m in Figure 7 (right; G1-piControl). Figure S7 shows the individual model results.

within ±50 m; the G1 model ensemble mean anomalies are less than 20 m relative to piControl (Figures 6 and S6). Generally, the G1 experiment maintains the geopotential at all height levels at its piControl magnitude (Figures 6 and 7). The spatial patterns of geopotential height anomalies G1-piControl are rather consistent across the models, with a larger intermodel scatter in winter than in other seasons. This may be caused by intermodel differences in surface thermal forcing and/or interaction with the baroclinic waves that affect planetary waves most strongly in winter.

Interestingly, the winter 500 hPa geopotential height response in four models (BNU-ESM, EC-EARTH, IPSL-CM5A-LR, and MPI-ESM-LR; Figure S6) represents a Pacific North America (PNA)-like pattern [*Wallace and Gutzler*, 1981]—a wave train over the North Pacific/North American region with opposite centers of action near the Aleutian Low in the Pacific; near Florida, southeast USA; and near Alberta, northern Canada. The PNA phase is however opposite between the experiments. The negative PNA phase is established in G1-piControl, while the positive phase of PNA is seen in abrupt4xCO2-piControl. Earlier simulations of future climate found varying responses [*Handorf and Dethloff*, 2009; *Hu et al*., 2001], and *Brandefelt and Körnich* [2008] found model-dependent responses which include positive and negative phases of PNA. They concluded that internal variability and intermodel differences play a role for the stationary wave response to the enhanced

greenhouse gas forcing. Generally, changes in PNA are related to changes in Rossby waves and their propagation conditions [e.g., *Hoskins and Karoly*, 1981; *Franzke et al*., 2011] and changes in heat sources such as tropical sea surface temperatures [*Hoskins and Karoly*, 1981; *Brandefelt*, 2006]. Tropical Pacific atmospheric temperature anomalies (e.g., generated by an in-phase combination of El Niño–Southern Oscillation and Pacific Decadal Oscillation) result in transfer of energy from the tropics toward North America, which helps maintain a PNA-like anomaly [e.g., *Yu and Zwiers*, 2007]. Thus, our result indicates that the G1 experiment is able to excite stationary waves, even though much weaker than in abrupt4xCO2, which might affect global teleconnection patterns. However, our G1 results also indicate across-model scatter in the magnitude of the 500 hPa geopotential height responses (Figures 6 and S6). The discussed changes in geopotential height are accompanied with upper tropospheric wind changes (Figures 7 and S7). The negative PNA-like pattern in G1-piControl is associated with a westward shift of the jet stream toward East Asia, blocking activity over the high latitudes of the North Pacific Ocean, and a strong split-flow configuration over the central North Pacific Ocean. Figure 7 displays these features with a decreased jet speed over central, west Pacific region (with across-model differences, Figure S7), and the 200 hPa geopotential height map also shows a "blocking" high pressure over the northern North Pacific under G1. In contrast, under abrupt4xCO2, the East Asian jet stream is intensified and eastward expanded. Our results are consistent with previous climate change studies which described a strengthening, broadening, and northward shift of the tropospheric zonal jets [e.g., *Lorenz and DeWeaver*, 2007; *Brandefelt and Körnich*, 2008] and with the findings of *Linkin and Nigam* [2008] that PNA is associated with strong fluctuations in the strength and location of the East Asian jet stream.

4. Mechanisms for Sea Ice Changes Under G1

As we have seen, the reductions in sea ice extent are dramatic in abrupt4xCO2 and much less so in the G1 scenario. However, there are clear regional differences in sea ice concentration under G1. Generally, changes in sea ice cover are a result of changes in temperature, winds, ocean currents and mixing, and surface heat fluxes. In the following, we discuss the most relevant processes.

4.1. Air Temperature Forcing

Figure 1 shows there are locations in the Arctic where G1 temperature response is much larger than the average ensemble response of 1°C warming. The anticorrelation between changes in surface air temperatures and sea ice concentrations is strongest in autumn (spatial pattern correlation coefficient $r = -0.6$ to -0.8) for all eight models (Table S2) and is suggestive of a strong degree of temperature control on sea ice concentrations. However, there is also the feedback between sea ice reduction and warmer temperatures that confounds attempts at determining causality. Regional differences in sea ice concentration in autumn under G1 (Figures 3 and S3), such as the reductions in Beaufort, Chukchi, East Siberian, Laptev Seas and the increase in the Barents Sea, approach 20%. The clear spatial correlations between sea ice concentration and surface air temperature changes in autumn expressed in Table S2 are also visible on regional scales by comparison of Figures 1 and 3 (and Figures S1 and S3 for the individual seasonal maps). Thus, these regional sea ice cover changes are plausibly related to temperature forcing.

In winter and spring, all models exhibit less spatial correlation between changes in surface air temperatures and sea ice concentrations under G1 (Table S2, eight model ensemble means of -0.34 and -0.3) compared with -0.72 for autumn. This reduction in temperature control can be explained as the ice coverage is high and air temperatures are well below freezing, implying that temperatures are not the limiting factor for sea ice cover near maximum ice extent. This suggests that changes in sea ice concentration during these seasons are governed more by atmospheric and/or oceanic forcing processes than radiative forcing (see following sections). In contrast, the abrupt 4xCO2 sea ice concentration changes are strongly spatially anticorrelated with temperature changes in all seasons (Table S3), with ensemble mean correlations of -0.83 in spring and -0.97 in autumn. This highlights the significant differences that the regional sea ice pattern changes in winter and spring under G1, which are much smaller than under abrupt4xCO2, are not directly forced by regional air temperatures.

4.2. Changed Sea Ice Drift

Under G1, in many models (BNU-ESM, GISS-E2-R, IPSL-CM5A-LR, MIROC-ESM, MPI-ESM-LR, and NorESM1-M) there is an increase in sea ice concentration in the Greenland Sea during March (Figure 3) and more generally

during winter and spring (see Figure S3). Temperature cannot be the main cause of this feature because only a small part of this region has reduced surface air temperatures (Figure S1). Hence, we suggest that changes in the sea ice drift path along the east Greenland current and the westerly Jan Mayen current cause, to some extent, this feature. These currents would draw the ice edge toward the west and give a large increase (from zero to 30%) in concentrations. Sea ice drift is determined by the atmospheric and oceanic shear stresses, caused by the wind and the ocean currents, respectively (but also depends on sea ice compactness). Because velocity data for neither sea ice nor ocean were available, we limit the discussion to the changes in near-surface wind and sea ice mass transport. The simulated near-surface wind anomaly in March shows an eastward (off-Greenland) directed flow (distinctive in IPSL-CM5A-LR and MPI-ESM-LR and weaker in BNU-ESM and MIROC-ESM; Figure 8) which is consistent with the sea ice increase in the Greenland Sea. This is also consistent with the ensemble mean surface wind anomaly in March that has an eastward component along southern Greenland. However, individual models show a fair degree of disagreement in wind direction (Figure 8), despite their agreement in the sea ice increase, so the mechanism may be more subtle. This increase in sea ice concentration seen at the east of Greenland under G1 in March is not caused by increased ice mass transport through the Fram Strait. Actually, Figure 8 shows that the ice mass transports are reduced (and Figure S8 shows that abrupt4xCO2 reduces even more), especially in the Fram Strait and the region south along East Greenland under G1 relative to piControl. This change amounts to about a 50% reduction in ice mass export from the Arctic relative to piControl. Reduced pack ice mass transport is consistent with the increase in relative importance of thinner first-year ice compared with multiyear ice under G1 (Table 1).

During summer and autumn, most models show reductions in G1 sea ice concentration in the Beaufort, Chukchi, East Siberian, and Laptev Seas of about 20% (Figures S3 and 3), which is largely temperature driven (section 4.1). And as the pack ice becomes looser, it can be transported more easily by the wind. Indeed, Figure 8 shows that the ensemble mean simulated sea ice mass transport under G1 is increased in these seas, although considerable across-model scatter occurs.

During March (and more generally during winter and spring), the models do not well agree on the Barents Sea sea ice concentration change under G1 (Figures 3 and S3). Generally, it has been shown that the sea ice extent in the Barents Sea is strongly coupled to the Atlantic water inflow [e.g., *Semenov*, 2008]. Hence, intermodel differences in ocean currents may help to explain why there is intermodel lack of agreement on Barents Sea ice concentration change under G1. But the analysis of ocean currents is beyond the scope of this paper. However, as we discuss in the next section, the cyclonic activity does change under G1, which would also impact the northward oceanic heat flux via the West Spitsbergen and Norwegian Atlantic Current, which bring Atlantic water into the Arctic and Barents Sea.

4.3. Change in Cyclonic Activity

As first suggested by *Blackmon* [1976] and following recent work [e.g., *Woollings et al*., 2012], we describe the cyclonic activity using the standard deviation of 2–6 day band-pass-filtered SLP (Figure 9). The 2–6 days filtering ensures that the storm track is restricted to the characteristic time scale of synoptic cyclones. This Eulerian definition of storm tracks is then defined as the region of enhanced standard deviation of filtered SLP. It is clear that cyclonic activity is changed under G1 in all seasons, with a high degree of disagreement in sign, magnitude, and pattern among the individual models (Figure 9, and in abrupt4xCO2, Figure S9). Thus, the cyclonic activity is not unaltered from piControl under G1. Accordingly, cyclone-driven sea ice modulation by warm air (and water) advection and/or sea ice advection can be expected. Thus, we seek to test the hypothesis that cyclonic activity changes under G1 relative to piControl, particularly across the Atlantic, can explain the changes in sea ice distribution in the Barents Sea in March (Figure 3) and more generally in winter and spring (Figure S3). Figure 9 shows model agreement on increased cyclonic activity entering the Barents Sea area in spring under G1 (see also Figure S9). Such a positive anomaly is associated with intensified poleward warm and moist air transport, consistent with the calculated regional sea ice reduction in the Barents Sea in the ensemble mean under G1 in March and spring. Based on the jet results (Figure 7), the simulated increase in 200 hPa zonal wind in G1-piControl indicates increased baroclinic instability and thus also points to an increased cyclonic activity in that region. Further, the baroclinic geopotential response (not shown) is an additional indication of increased cyclonic activity in that region in spring.

It should be noted that causality is difficult to determine here. In discussing the impact of cyclones on sea ice, it must also be considered that the sea ice edge guides cyclones. Sea ice anomalies impact the low-level

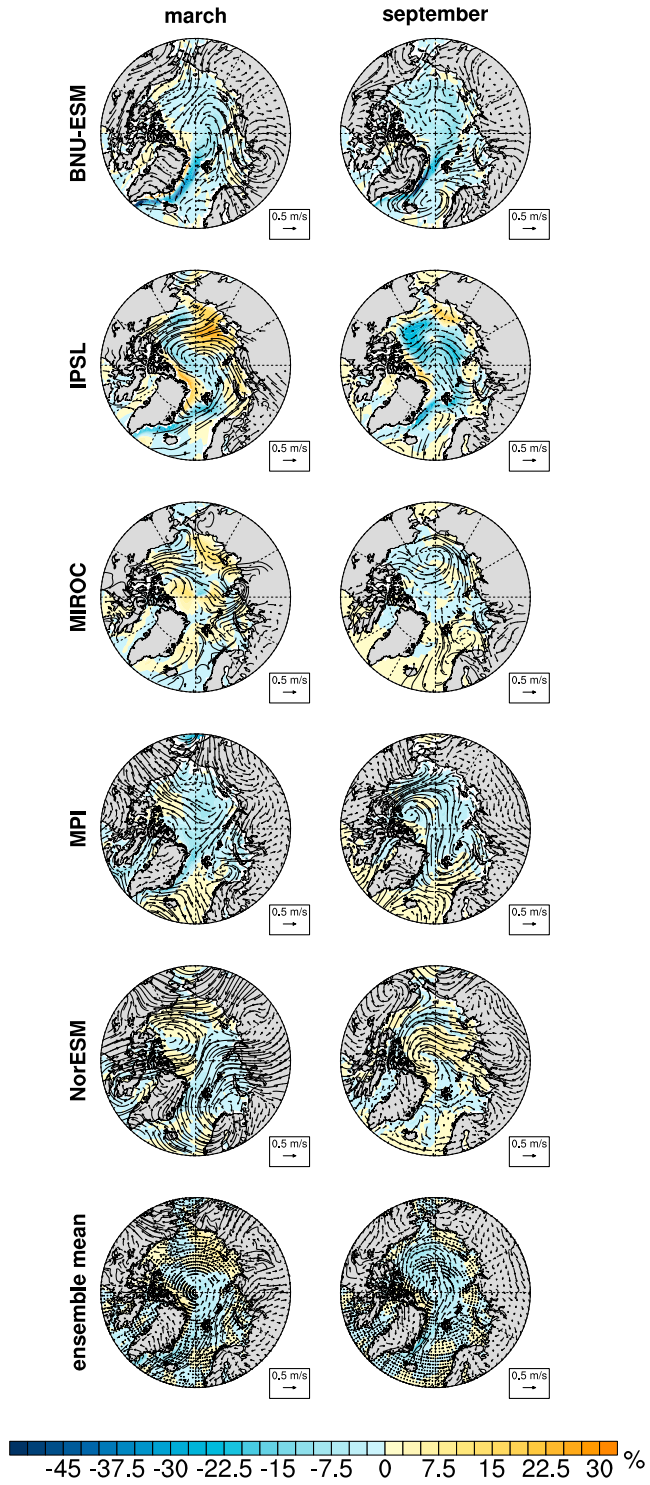

Figure 8. Individual model and multimodel ensemble mean sea ice mass transport (kg/s; color) and near-surface wind (m/s; arrows) anomalies for G1-piControl for March and September. Mass transport anomalies are calculated relative to the maximum transport in piControl. CCSM, EC-EARTH, and GISS data were not available. The ensemble mean has stippling where less than four of five models agree on the sign of change. Figure S8 shows the abrupt4xCO2 anomalies.

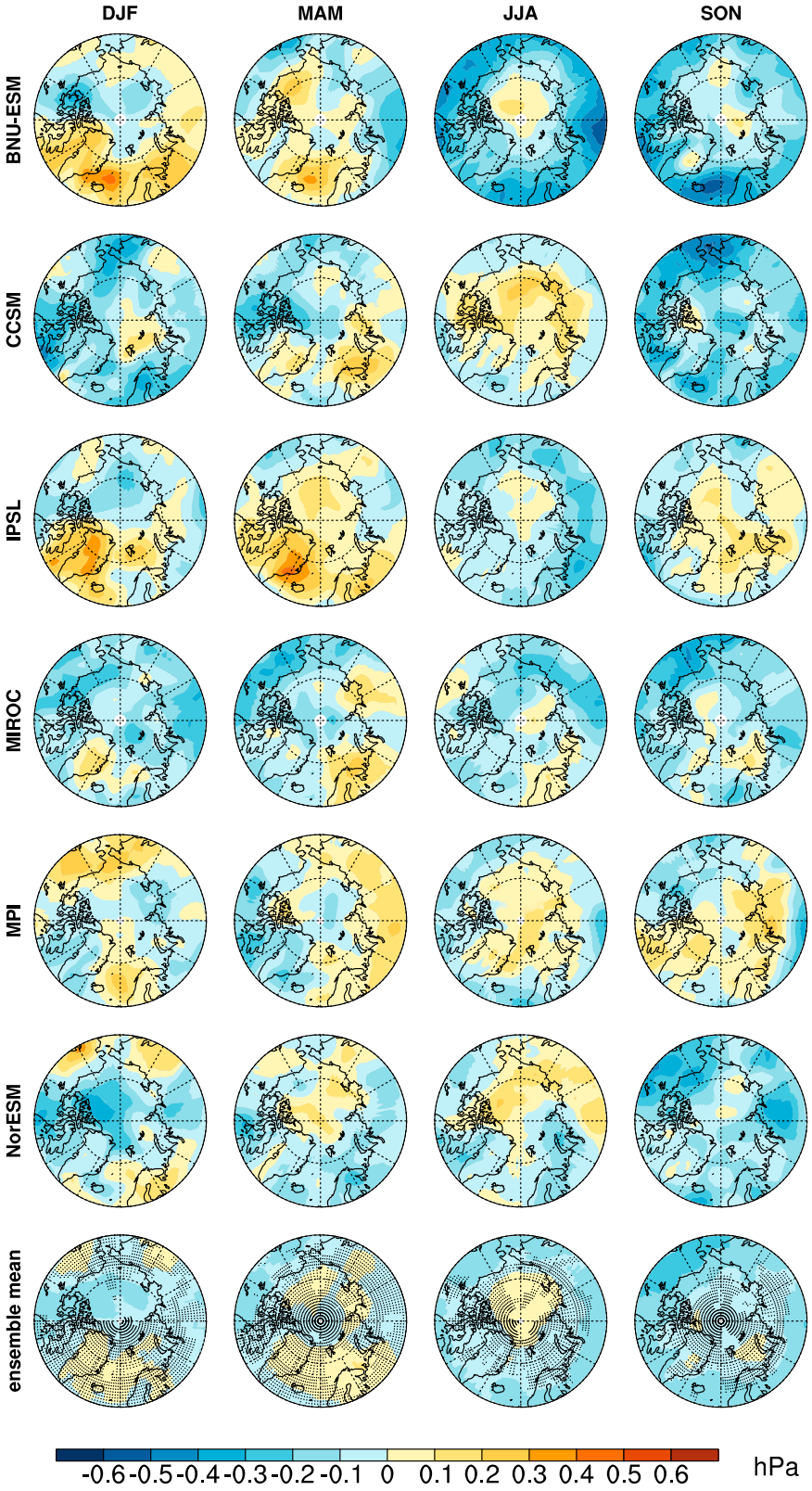

Figure 9. Individual model and multimodel ensemble mean standard deviation of 2–6 days filtered sea level pressure data (hPa) for G1-piControl for the four seasons. EC-EARTH and GISS data were not available. The ensemble mean has stippling where less than five of six models agree on the sign of change. Figure S9 shows the abrupt4xCO2 anomalies.

baroclinicity and accordingly the path and intensity of storms; sea ice reduction displaces temperature gradients and force storm tracks to be diverted northward [e.g., *Zhang et al*., 2008; *Budikova*, 2009; *Wu and Zhang*, 2010; *Inoue et al*., 2012]. Hence, it is more appropriate to consider mechanisms as feedback rather than causes and effects.

5. Conclusions and Implications

To a crude approximation, G1 returns Arctic sea ice concentrations and extent to preindustrial conditions with intermodel spread of seasonal ice extent being much greater than the difference in ensemble means of preindustrial and G1. However, there are significant and intermodel consistent differences in sea ice seasonal distribution, which are related to both changes in surface temperatures and atmospheric and oceanic circulation. In winter and spring, sea ice reduction in the Barents Sea has been, in addition to temperature changes, related to increased North Atlantic cyclonic activity, while sea ice increase in the Greenland Sea seems to be associated with ice drift changes. In summer and autumn, air temperature forcing is the main factor for regional sea ice changes, although changes in cyclonic activity and ice drift play a role too.

The predicted sea ice concentration changes are particularly large in the Beaufort, Chukchi, East Siberian, and Laptev Seas. These regions contain indigenous populations whose traditional activities will be impacted by sea ice changes [*AHDR*, 2004]. They also contain gas hydrates which may play an important feedback role to climate change if the vast quantities of methane are thawed as the Arctic Ocean warms [*Shakhova et al*., 2010]. However, the changes are far smaller than the transition to a virtually summer sea ice free Arctic Ocean condition that is likely under abrupt4xCO2 forcing. Arctic sea ice projections by the end of the 21st century are most sensitive to the prescribed greenhouse gas forcing, and the sea ice changes can be limited by mitigation of greenhouse gas emissions. For the RCP2.6 scenario (*Moss et al*., 2010 aggressive mitigation or even implicit geoengineering by CO_2 removal), only a slight decrease in sea ice concentration is simulated. Under a medium emission scenario (RCP4.5) sea ice decline is strong but not as rapid as under the RCP8.5 scenario. Many models show sea ice remaining at more than 2 million km^2 under RCP4.5, while the majority of the models simulate nearly ice-free conditions under RCP8.5 by the end of this century [*Stroeve et al*., 2012; *Massonnet et al*., 2012].

The nature of feedback between surface temperature, sea ice, and atmospheric circulation means that determining causal relations is challenging. The change under G1 of the drift pack along the east Greenland current and the northward change of the storm track into the Barents Sea in most models suggests that even with the modest change in net radiative forcing under G1 there will be impacts on atmospheric and ocean circulation patterns that can have disproportionate impacts. For example, changes in iceberg lanes in the Atlantic may impact shipping routes. Under projected 21st century climate forcing CO_2 levels only approach the quadrupling of CO_2 levels with RCP8.5 (1370 ppm CO_2 equivalent) in 2100 [*Moss et al*., 2010]. *Kravitz et al*. [2013b] estimate that under G1, a shortwave forcing of about 6 Wm^{-2} at the surface would be needed to counteract quadrupling of CO_2. This is more than normally considered in geoengineering scenarios [e.g., *Moore et al*., 2010] and extremely challenging by solar dimming (about 3% of solar insolation), but if done by stratospheric sulfate aerosols then the mass needed would be a few times larger than that already lifted close to the tropopause by commercial aircraft each year. However, this is not designed to be a realistic scenario but rather a way of informing on extreme future changes. A relatively ice-free summer would then mean that the open water Northern Sea route would likely become an important trade route between Europe and Asia, impacting other global routes such as those through the Suez and Panama Canals. However, the reduction (but not removal) of Arctic pack ice would encourage less capable shipping to undertake the Northern Sea route, leading to greater risk of shipping accidents along Arctic coasts which are particularly vulnerable to ecological damage [*Forbes*, 2011].

Acknowledgments
We thank all participants of the Geoengineering Model Intercomparison Project and their model development teams, the CLIVAR/WCRP Working Group on Coupled Modeling for endorsing GeoMIP, the scientists managing the Earth System Grid data nodes who have assisted with making GeoMIP output available. We acknowledge the World Climate Research Programme's Working Group on Coupled Modelling, which is responsible for CMIP, and we thank the climate modeling groups (listed in Table S1) for producing and making available their model output. For CMIP, the U.S. Department of Energy's Program for Climate Model Diagnosis and Intercomparison provides coordinating support and led development of software infrastructure in partnership with the Global Organization for Earth System Science Portals. D.J., X.Y., X.C., and J.C.M. thank all members of the BNU-ESM model group and support from the Joint Center for Global Change Studies (JCGCS), as well as the Center of Information and Network Technology at Beijing Normal University for assistance in publishing the GeoMIP data set. B.K. is supported by the Fund for Innovative Climate and Energy Research. Simulations performed by B.K. were supported by the NASA High-End Computing (HEC) Program through the NASA Center for Climate Simulation (NCCS) at Goddard Space Flight Center. K.A., J.E.K., U.N., H.S., O.B., and M.S. received funding from the European Union's Seventh Framework Programme (FP7/2007–2013) under the IMPLICC project (grant 226567) and the EuTRACE project (grant 306395). K.A. and J.E.K. received support from the Norwegian Research Council's Programme for Supercomputing (NOTUR) through a grant of computing time. Simulations with the IPSL-CM5 model were supported through HPC resources of [CCT/TGCC/CINES/IDRIS] under the allocation 2012-t2012012201 made by GENCI (Grand Equipement National de Calcul Intensif). The National Center for Atmospheric Research is funded by the National Science Foundation (NSF). S.W. was supported by the SOUSEI program, MEXT, Japan, and his simulations were performed using the Earth Simulator. Alan Robock is supported by NSF grants AGS-1157525 and CBET-1240507.

References

Arctic Human Development Report (AHDR) (2004), *Arctic Human Development Report*, pp. 242, Stefansson Arctic Institute, Akureyri.
Arctic Monitoring and Assessment Programme (2007), *Arctic Monitoring and Assessment Programme, Arctic Oil and Gas*, pp. 40, AMAP, Oslo.
Bindoff, N. L., et al. (2007), Observations: Oceanic climate change and sea level, in *Climate Change 2007: The Physical Science Basis. Contribution of Working Group I to the Fourth Assessment Report of the Intergovernmental Panel on Climate Change*, edited by S. Solomon et al., pp. 385–432, Cambridge Univ. Press, Cambridge, United Kingdom and New York, NY, USA.
Blackmon, M. L. (1976), A climatological spectral study of the 500 mb geopotential height of the Northern Hemisphere, *J. Atmos. Sci.*, *33*, 1607–1623.
Brandefelt, J. (2006), Atmospheric modes of variability in a changing climate, *J. Clim.*, *19*, 5934–5943.
Brandefelt, J., and H. Körnich (2008), Northern Hemisphere stationary waves in future climate projections, *J. Clim.*, *21*, 6341–6353.

Budikova, D. (2009), Role of Arctic sea ice in global atmospheric circulation: A review, *Global Planet. Change*, *68*(2009), 149–163.
Cohen, J. L., J. C. Furtad, M. A. Barlow, V. A. Alexeev, and J. E. Cherry (2012), Arctic warming, increasing snow cover and widespread boreal winter cooling, *Environ. Res. Lett.*, *7*, doi:10.1088/1748-9326/7/1/014007.
Dethloff, K., et al. (2006), A dynamical link between the Arctic and the global climate system, *Geophys. Res. Let.*, *33*, L03703, doi:10.1029/2005GL025245.
Forbes, D. L. (Ed.) (2011), *State of the Arctic Coast 2010 – Scientific Review and Outlook. International Arctic Science Committee, Land-Ocean Interactions in the Coastal Zone, Arctic Monitoring and Assessment Programme, International Permafrost Association*, pp. 178, Helmholtz-Zentrum, Geesthacht, Germany.
Francis, J. A., and S. J. Vavrus (2012), Evidence linking Arctic amplification to extreme weather in midlatitudes, *Geophys. Res. Lett.*, *39*, L06801, doi:10.1029/2012GL051000.
Franzke, C., S. B. Feldstein, and S. Lee (2011), Synoptic analysis of the Pacific-North American teleconnection pattern, *Q. J. R. Meteorol. Soc.*, *137*, 329–346.
Handorf, D., and K. Dethloff (2009), Atmospheric teleconnections and flow regimes under future climate projections, *Eur. Phys. J. Spec. Top.*, *174*, 237–255, doi:10.1140/epjst/e2009-01104-9.
Honda, M., J. Inoue, and S. Yamane (2009), Influence of low Arctic sea-ice minima on anomalously cold Eurasian winters, *Geophys. Res. Lett.*, *36*, L08707, doi:10.1029/2008GL037079.
Hoskins, B. J., and D. J. Karoly (1981), The steady linear response of a spherical atmosphere to thermal and orographic forcing, *J. Atmos. Sci.*, *38*, 1179–1196.
Hu, Z.-Z., L. Bengtsson, E. Roeckner, M. Christoph, A. Bacher, and J. Oberhuber (2001), Impact of global warming on the interannual and interdecadal climate modes in a coupled GCM, *Clim. Dyn.*, *17*, 361–374.
Inoue, J., M. E. Hori, and K. Takaya (2012), The role of Barents Sea ice in the wintertime cyclone track and emergence of a warm-Arctic cold-Siberian anomaly, *J. Clim.*, *25*, 2561–2568.
Jaiser, R., K. Dethloff, D. Handorf, A. Rinke, and J. Cohen (2012), Impact of sea ice cover changes on the Northern Hemisphere atmospheric winter circulation, *Tellus A*, *64*, 11,595, doi:10.3402/tellusa.v64i0.11595.
Kravitz, B., A. Robock, O. Boucher, H. Schmidt, and K. E. Taylor (2011a), Specifications for GeoMIP experiments G1 through G4 (Version 1.0). [Available at http://climate.envsci.rutgers.edu/GeoMIP/docs/specificationsG1_G4_v1.0.pdf.]
Kravitz, B., A. Robock, O. Boucher, H. Schmidt, K. E. Taylor, G. Stenchikov, and M. Schulz (2011b), The Geoengineering Model Intercomparison Project (GeoMIP), *Atmos. Sci. Lett.*, *12*, 162–167, doi:10.1002/asl.316.
Kravitz, B., et al. (2013a), Climate model response from the Geoengineering Model Intercomparison Project (GeoMIP), *J. Geophys. Res. Atmospheres*, *118*, 8320–8332, doi:10.1002/jgrd.50646.
Kravitz, B. K., et al. (2013b), An energetic perspective on hydrologic cycle changes in the Geoengineering Model Intercomparison Project (GeoMIP), *J. Geophys. Res. Atmospheres*, *118*, 13,087–13,102, doi:10.1002/2013JD020502.
Linkin, M. E., and S. Nigam (2008), The North Pacific Oscillation–West Pacific teleconnection pattern: Mature-phase structure and winter impacts, *J. Clim.*, *21*, 1979–1997, doi:10.1175/2007JCLI2048.1.
Liu, J., J. A. Curry, H. Wang, M. Song, and R. M. Horton (2012), Impact of declining Arctic sea ice on winter snowfall, *Proc. Natl. Acad. Sci. U. S. A.*, *109*, 4074–4079, doi:10.1073/pnas.1114910109.
Lorenz, D. J., and E. T. DeWeaver (2007), Tropopause height and zonal wind response to global warming in the IPCC scenario integrations, *J. Geophys. Res.*, *112*, D10119, doi:10.1029/2006JD008087.
Maslowski, W., J. C. Kinney, M. Higgins, and A. Roberts (2012), The future of Arctic sea ice, *Annu. Rev. Earth Planet. Sci.*, *40*, 625–654, doi:10.1146/annurev-earth-042711-105345.
Massonnet, F., T. Fichefet, H. Goosse, C. M. Bitz, G. Philippon-Berthier, M. M. Holland, and P.-Y. Barriat (2012), Constraining projections of summer Arctic sea ice, *Cryosphere*, *6*, 1383–1394, doi:10.5194/tc-6-1383-2012.
McCusker, K. E., D. S. Battisti, and C. M. Bitz (2012), The climate response to stratospheric sulfate injections and implications for addressing climate emergencies, *J. Clim.*, *25*, 3096–3116, doi:10.1175/JCLI-D-11-00183.1.
Moore, J. C., S. Jevrejeva, and A. Grinsted (2010), Efficacy of geoengineering to limit 21st century sea-level rise, *Proc. Natl. Acad. Sci. U. S. A.*, doi:10.1073/pnas.1008153107.
Moss, R. H., et al. (2010), The next generation of scenarios for climate change research and assessment, *Nature*, *463*, 747–756.
Ogi, M., I. G. Rigor, M. G. McPhee, and J. M. Wallace (2008), Summer retreat of Arctic sea ice: Role of summer winds, *Geophys. Res. Lett.*, *35*, L24701, doi:10.1029/2008GL035672.
Overland, J. E., and M. Wang (2010), Large-scale atmospheric circulation changes are associated with the recent loss of Arctic sea ice, *Tellus A*, *62*, 1–9, doi:10.1111/j.1600-0870.2009.00421.x.
Petoukhov, V., and V. A. Semenov (2010), A link between reduced Barents-Kara sea ice and cold winter extremes over northern continents, *J. Geophys. Res.*, *115*, D21111, doi:10.1029/2009JD013568.
Richter-Menge, J., and J. E. Overland (Eds.) (2010), Arctic Report Card 2010. [Available at http://www.arctic.noaa.gov/reportcard.]
Rinke, A., K. Dethloff, W. Dorn, D. Handorf, and J. C. Moore (2013), Simulated Arctic atmospheric feedbacks associated with late summer sea ice anomalies, *J. Geophys. Res. Atmospheres*, *118*, 7698–7714, doi:10.1002/jgrd.50584.
Schröder, D., and W. M. Connolley (2007), Impact of instantaneous sea ice removal in a coupled general circulation model, *Geophys. Res. Let*, *34*, L14502, doi:10.1029/2007GL030253.
Screen, J. A., I. Simmonds, C. Deser, and R. Tomas (2013), The atmospheric response to three decades of observed Arctic sea ice loss, *J. Clim.*, *26*, 1230–1248, doi:10.1175/JCLI-D-12-00063.1.
Semenov, V. A. (2008), Influence of oceanic inflow to the Barents Sea on climate variability in the Arctic region, *Dokl. Earth Sci.*, *418*, 91–94, doi:10.1134/S1028334X08010200.
Shakhova, N., I. Semiletov, A. Salyuk, V. Yusupov, D. Kosmach, and Ö. Gustafsson (2010), Extensive methane venting to the atmosphere from sediments of the East Siberian Arctic Shelf, *Science*, *327*, 1246–1250.
Stroeve, J., V. Kattsov, A. P. Barrett, M. Serreze, T. Pavlova, M. Holland, and W. Meier (2012), Trends in Arctic sea ice extent from CMIP5, CMIP3 and observations, *Geophys. Res. Lett.*, *39*, L16502, doi:10.1029/2012GL052676.
Tang, Q., X. Zhang, X. Yang, and J. A. Francis (2013), Cold winter extremes in northern continents linked to Arctic sea ice loss, *Environ. Res. Lett.*, *8*, 014,036, doi:10.1088/1748-9326/8/1/014036.
Taylor, K. E., R. J. Stouffer, and G. A. Meehl (2012), An overview of CMIP5 and the experiment design, *Bull. Am. Meteorol. Soc.*, *93*, 485–498, doi:10.1175/BAMS-D-11-00094.1.
Wallace, J. M., and D. Gutzler (1981), Teleconnections in the geopotential height field during the Northern Hemisphere winter, *Mon. Weather Rev.*, *109*, 784–812.

Wang, M., and J. E. Overland (2012), A sea ice free summer Arctic within 30 years: An update from CMIP5 models, *Geophys. Res. Lett.*, *39*, L18501, doi:10.1029/2012GL052868.

Woollings, T., J. M. Gregory, J. G. Pinto, M. Reyers, and D. J. Brayshaw (2012), Response of the North Atlantic storm track to climate change shaped by ocean-atmosphere coupling, *Nat. Geosci.*, *5*, doi:10.1038/ngeo1438.

Wu, Q., and X. Zhang (2010), Observed forcing-feedback processes between Northern Hemisphere atmospheric circulation and Arctic sea ice coverage, *J. Geophys. Res.*, *115*, D14119, doi:10.1029/2009JD013574.

Yu, B., and F. W. Zwiers (2007), The impact of combined ENSO and PDO on the PNA climate: A 1000-yr climate modeling study, *Clim. Dyn.*, *29*, 837–851, dos:10.1007/s00382-007-0267-4.

Zhang, X., and J. E. Walsh (2006), Toward a seasonally ice-covered Arctic Ocean: Scenarios from the IPCC AR4 model simulations, *J. Clim.*, *19*, 1730–1747, doi:10.1175/JCLI3767.1.

Zhang, X., A. Sorteberg, J. Zhang, R. Gerdes, and J. C. Comiso (2008), Recent radical shifts of atmospheric circulations and rapid changes in Arctic climate system, *Geophys. Res. Lett.*, *35*, L22701, doi:10.1029/2008GL035607.